

Elastic response of a grounded ice sheet coupled to a floating ice shelf

Roiy Sayag* and M. Grae Worster

Institute of Theoretical Geophysics, Department of Applied Mathematics and Theoretical Physics, University of Cambridge, Cambridge CB3 0WA, United Kingdom

(Received 28 April 2011; published 19 September 2011)

An ice sheet that spreads into an ocean is forced to bend owing to its buoyancy and detaches from the bedrock to form a floating ice shelf. The location of the transition between the grounded sheet and the floating shelf, defined as the grounding line, behaves as a free boundary. We develop a model of an elastic grounded sheet resting on a deformable elastic bed and coupled to an elastic floating shelf. We find that the grounding-line position is determined by the geometry of the bed and the bending-buoyancy length scale of the system. These two contributions depend on the reaction modulus of the bed in opposite ways. We show that the structure of the floating shelf depends on the bending-buoyancy length scale only, allowing us to calculate the bending stiffness of the elastic sheet independently of the properties of the bed. Relations between the structure of the floating shelf and the grounding-line position are also developed. Our theoretical predictions agree with laboratory experiments made using thick elastic sheets and a dense salt solution. Our findings may provide new insights into the dynamics near grounding lines, as well as methods to infer the bending stiffness of ice sheets and the grounding-line position from satellite altimetry that can be applied to elastic sheets in general.

DOI: [10.1103/PhysRevE.84.036111](https://doi.org/10.1103/PhysRevE.84.036111)

PACS number(s): 62.20.D-, 92.40.vv, 83.80.Nb, 42.68.Wt

I. INTRODUCTION

An ice sheet that extends into an ocean is composed of one part that is grounded to the underlying bed and another part that is detached from the bed to become a floating ice shelf. The force balance near the line that joins these two parts and the bed, known as the grounding line, may be related to instabilities of steady marine ice sheets [1] and consequently to abrupt change in sea level.

The position of the grounding line is determined by the interactions between the ice, the ocean, and the underlying bed. The major dynamic contribution of the ocean is through the buoyancy force it exerts on the ice, while the bed underneath the ice, which has composition that varies from stiff rock to deformable mixture of water and sediments, may act as an elastic cushion [2] that supports the weight of the ice sheet. The response of the ice, which may be reflected through its surface geometry near the grounding line, depends on the dominant rheology of the ice. Specifically, in the vicinity of the grounding line, the surface of the ice often has an undulated structure with a length scale of several kilometers, e.g. [3]. Such undulations can be explained by continuum models employing a range of rheologies from elastic to viscous [4–12]. Here, we consider the deformation of a purely elastic sheet, noting that this is relevant to cases in which the transit time of ice across an undulation is short compared to the viscous relaxation time scale [13].

Conceptually, the grounded sheet and the floating shelf can be modelled separately, with the grounding line being a free boundary in between. This is analogous to a Stefan problem for solidifying boundaries [14], which requires an additional (Stefan) condition to resolve the free boundary. However, such a boundary condition for grounding lines is not known *a priori*. A common assumption is that the ice thickness at the grounding line satisfies Archimedean balance, yet viscous ice

models that assume that balance do not resolve the undulated structure of the grounded zone, e.g. [15–17]. Other viscous ice models that do not assume Archimedean balance at the grounding line do resolve an undulated structure on the side of the floating shelf [4–7]. Studies that model ice as an elastic or viscoelastic material also resolve an undulated structure, yet these have typically included only the floating ice shelf and treated the grounding line as a fixed boundary, e.g. [8–12].

We analyze a coupled model for an elastic sheet-shelf system, in which the grounding line is treated as a free boundary. The bed beneath the grounded sheet has a softness parameter that can be physically interpreted as a foundation modulus [18]. This accounts for the observed features of ice-sheet beds and also allows smoother transition of the reaction forces across the grounding line. We present analytical and numerical solutions for the deflection profiles and for the grounding-line position and we verify some theoretical predictions using a laboratory scale experiment (Fig. 1).

Although motivated by marine ice shelves, our theory is developed in complete generality for an elastic sheet supported in part by an elastic solid and in part by a denser fluid.

II. MATHEMATICAL MODEL

Consider an elastic sheet of thickness H , density ρ_i , and bending stiffness D that is positioned on a bed that is partially immersed in an ocean of density $\rho_w > \rho_i$, as illustrated in Fig. 2. The bed may represent a soil that is allowed to deform according to a linear elastic model (Winkler foundation) with a modulus of subgrade reaction k_0 . The intersection of the ocean surface with the bed is the position $x = 0$, where the x coordinate is along the undisturbed ocean surface and the y coordinate is positive upward. The bed has an undisturbed profile $y_b(x) = -Sx$, where $\tan^{-1} S$ is the angle that the undeformed bed makes with the horizontal. Hydrostatic pressure on the immersed part of the sheet causes it to bend and detach from the bed to form a shelf, with a grounding line at $x = x_g$.

*r.sayag@damtp.cam.ac.uk

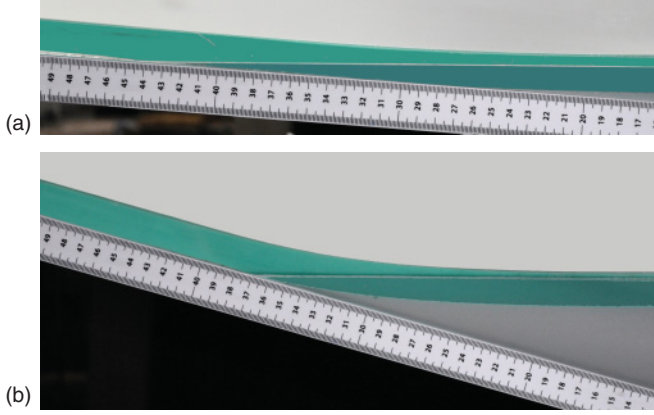


FIG. 1. (Color online) Images of the grounding zone formed with a 2-cm elastic sheet and a 1.52-g/cm^3 ocean for a $\sim 3.7^\circ$ bed inclination (a), where the free surface of the ocean fluid intersects the bed at 44 cm and the grounding line is below it near 31 cm, and for a $\sim 15^\circ$ bed inclination (b), where the free surface of the ocean fluid intersects the bed at 37 cm and the grounding line is above it near 42 cm.

Mathematically, this situation can be modelled using the Euler-Bernoulli beam equation,

$$D \frac{d^4 y}{dx^4} = p(x, y), \quad (1)$$

where y is the deflection of the center line of the sheet from the ocean free surface, $p(x, y)$ is the load on the sheet, and

$$D = \frac{EH^3}{12(1-\nu^2)}, \quad (2)$$

where ν is the Poisson ratio and E is Young's elastic modulus. Equation (1) is valid for a slender sheet having a small thickness compared with the minimum radius of curvature and a uniform bending stiffness and assuming that longitudinal stretching is negligible compared with bending. We also constrain the analysis to the case where the shelf surface is everywhere above the ocean surface.

A. Grounding line below the surface of the ocean

We first consider the case where the grounding line is below the surface of the ocean. We identify two regions that meet at x_g (Fig. 2, top): a grounded region, $x \leq x_g$ (in full contact with the bed), and an ungrounded region, $x > x_g$ (detached). The vertical force balance in each region is

$$Dy^{iv} = -\rho_i g H + k_0(H/2 - y + y_b) \quad x_f \leq x \leq x_g, \quad (3a)$$

$$Dy^{iv} = -\rho_i g H + \rho_w g(H/2 - y) \quad x_g < x \leq x_s, \quad (3b)$$

where the second term on the right-hand side of each equation represents the restoring force applied by the bed (3a) or by the ocean (3b), as appropriate. Equations (3) are a set of two fourth-order ordinary differential equations (ODE's) with two free parameters; the position of the grounding line x_g and the

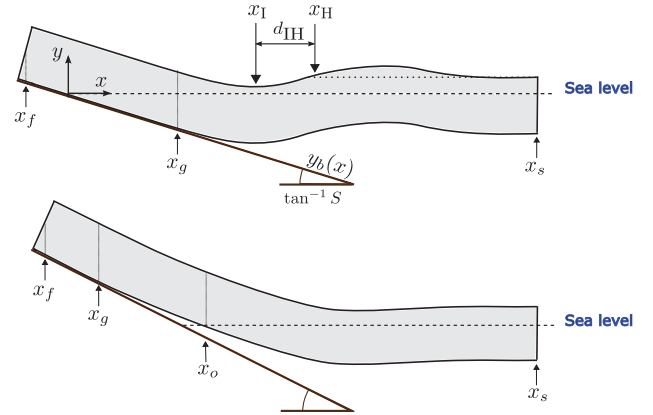


FIG. 2. (Color online) Schematic diagrams of the vertical cross section of a sheet-shelf system near the grounding line. For a bed profile y_b of shallow angles $\tan^{-1} S$ (top panel), the grounding line x_g is below the ocean free surface (dashed line). The same sheet-shelf at larger angles (bottom panel) can have a grounding line above the free surface. In the latter situation there is a free boundary within the floating shelf at the position x_o where it penetrates the ocean. The position x_I marks a local minimum of the shelf elevation, and the position x_H is the nearest point down from x_I where ice elevation equals the hydrostatic value (dotted line). The position $x = 0$ is where sea level intersects with the bed.

position of the shelf edge x_s . The 10 boundary conditions required to close the problem are

$$y = H \left(\frac{1}{2} - \frac{\rho_i g}{k_0} \right) + y_b(x) \quad x = x_f, \quad (4a)$$

$$y' = y'_b(x) \quad x = x_f, \quad (4b)$$

$$[y] = [y'] = [y''] = [y'''] = 0 \quad x = x_g, \quad (4c)$$

$$y = H/2 + y_b \quad x = x_g, \quad (4d)$$

$$y'' = y''' = 0 \quad x = x_s, \quad (4e)$$

along with a constraint on the total arclength of the sheet,

$$\int_{x_f}^{x_s} \sqrt{1 + y'^2} dx = L, \quad (5)$$

where L is given. The interpretation of Eqs. (4a) and (4b) is that x_f is sufficiently far from the grounding zone that the edge of the grounded sheet behaves as if there is no shelf. In fact, imposing these two boundary conditions at $x_f \rightarrow -\infty$ has a negligible effect on the results but simplifies the calculation. Across the grounding line we assume continuity of position, slope, bending moment, and shear force (4c); at the grounding line the shelf is grounded (4d) and the shelf edge is free (4e). The conditions above are slightly modified when we consider the long-shelf limit, $L \rightarrow \infty$. In that case, $x_s \rightarrow \infty$ so there is one fewer free boundary and therefore the boundary conditions (4) are sufficient to close the system (3).

We nondimensionalize using

$$\hat{y}_i = y_i/H, \quad (6)$$

where the subscript $i = 0, 1$ refers to the grounded part and the floating part, respectively, which leads to (hats removed)

$$y_0^{iv} = -4\gamma_0^4 \left(y_0 - \frac{1}{2} + \frac{\rho_i g}{k_0} - y_b \right), \quad (7a)$$

$$y_1^{iv} = -4\gamma_1^4 \left(y_1 - \frac{1}{2} + \rho_{iw} \right), \quad (7b)$$

where $y_b(x) = -S \frac{x}{H}$, $\rho_{iw} = \rho_i / \rho_w$ and

$$\gamma_0 = \frac{1}{l\sqrt{2}} \left(\frac{k_0}{\rho_w g} \right)^{1/4} = \frac{1}{\sqrt{2}} \left(\frac{k_0}{D} \right)^{1/4}, \quad (8a)$$

$$\gamma_1 = \frac{1}{l\sqrt{2}}, \quad (8b)$$

with the bending-buoyancy length scale

$$l = \left(\frac{D}{\rho_w g} \right)^{1/4}, \quad (9)$$

which depends on the bending stiffness of the sheet and the buoyancy per unit volume of the surrounding fluid. Note that the length scale γ_0^{-1} depends only on the bending stiffness of the sheet and the reaction modulus of the bed.

The solution to Eqs. (7a) and (7b) has the general form $y_i = y_{ih} + y_{ip}$, where

$$y_{0p} = \frac{1}{2} - \frac{\rho_i g}{k_0} + y_b, \quad (10a)$$

$$y_{1p} = \frac{1}{2} - \rho_{iw}, \quad (10b)$$

representing a sheet resting on a bed with no shelf (10a) and an iceberg (10b) and where the homogeneous solution is

$$y_{ih} = e^{\gamma_i x} [a_{i1} \cos(\gamma_i x) + a_{i2} \sin(\gamma_i x)] + e^{-\gamma_i x} [a_{i3} \cos(\gamma_i x) + a_{i4} \sin(\gamma_i x)], \quad (11)$$

with the coefficients a_{ij} and the unknown free boundaries x_g, x_s determined by the boundary conditions.

B. Grounding line above the surface of the ocean

A grounding line above the surface of the ocean (Fig. 2, bottom) is not realistic in natural ice sheets. Nevertheless, it is a natural continuation to the configuration in Sec. II A and we use it in the experimental validation of the theory in Sec. IV. In this configuration, there is additional ungrounded region between the partially submerged shelf and the grounded sheet, where the shelf is above the ocean surface. The vertical force balance at each of those regions is then

$$Dy^{iv} = -\rho_i g H + k_0(H/2 - y + y_b) \quad x_f \leq x \leq x_g, \quad (12a)$$

$$Dy^{iv} = -\rho_i g H \quad x_g < x \leq x_o, \quad (12b)$$

$$Dy^{iv} = -\rho_i g H + \rho_w g(H/2 - y) \quad x_o < x \leq x_s, \quad (12c)$$

where x_o represents the contact point of the shelf with the ocean surface. The system (12) is a set of three fourth-order ODE's with three free parameters, x_g, x_o , and x_s , therefore

15 boundary conditions are required to close the problem. Following the same arguments as in Sec. II A we set,

$$y = H \left(\frac{1}{2} - \frac{\rho_i g}{k_0} \right) + y_b(x) \quad x = x_f, \quad (13a)$$

$$y' = y'_b(x) \quad x = x_f, \quad (13b)$$

$$[y] = [y'] = [y''] = [y'''] = 0 \quad x = x_g, \quad (13c)$$

$$y = H/2 + y_b \quad x = x_g, \quad (13d)$$

$$[y] = [y'] = [y''] = [y'''] = 0 \quad x = x_o, \quad (13e)$$

$$y = H/2 \quad x = x_o, \quad (13f)$$

$$y'' = y''' = 0 \quad x = x_s, \quad (13g)$$

along with the constraint (5). We nondimensionalize as before to obtain

$$y_0^{iv} = -4\gamma_0^4 \left(y_0 - \frac{1}{2} + \frac{\rho_i g}{k_0} - y_b \right), \quad (14a)$$

$$y_1^{iv} = -4\bar{\gamma}_1^4, \quad (14b)$$

$$y_2^{iv} = -4\gamma_2^4 \left(y_2 - \frac{1}{2} + \rho_{iw} \right), \quad (14c)$$

where now

$$\bar{\gamma}_1 = \frac{1}{l\sqrt{2}} \rho_{iw}^{1/4}, \quad \gamma_2 = \frac{1}{l\sqrt{2}}, \quad (15)$$

with the subscripts 0, 1, and 2 referring to the grounded part of the sheet and the two shelf parts, respectively. The solutions to y_0 and y_2 have identical form to the solutions for y_0 and y_1 in Sec. II A, while the solution for y_1 is

$$y_1 = -\frac{1}{3!} \bar{\gamma}_1^4 x^4 + a_{13} x^3 + a_{12} x^2 + a_{11} x + a_{10}, \quad (16)$$

where $x_g \leq x \leq x_o$ and a_{1j} are constants that are chosen to satisfy the boundary conditions.

III. RESULTS

The models described in Secs. II A and II B have a nonlinear component due to the finite length of the shelf, introduced through constraint (5). This requires solving the models numerically. However, in the limit of a long shelf ($x_s - x_g \rightarrow \infty$) the edge of the shelf x_s is no longer modelled as a free boundary and therefore the length constraint (5) is not required, making it simpler to attain analytical solutions. Below, we present an analytical solution for the case of a grounding line below sea level (Sec. II A) and results from numerical solutions for a system of finite length and for the case where the grounding line is above the ocean free surface.

A. Solutions in the long shelf limit

The solution of the grounded sheet in the limit of a long shelf and for the case $x_g > 0$ is

$$y_0 = \frac{1}{2} - \frac{\rho_i g}{k_0} - \frac{Sx}{H} + e^{\gamma_0(x-x_g)} \left\{ \cos[\gamma_0(x-x_g)] \frac{\rho_i g}{k_0} + \frac{\sin[\gamma_0(x-x_g)]}{1 + \frac{\gamma_1}{\gamma_0}} \left[\frac{\rho_i g}{k_0} + \frac{\gamma_1^3}{\gamma_0^3} \left(\rho_{iw} - \frac{Sx_g}{H} \right) \right] \right\}, \quad (17)$$

which is a superposition of a flat sheet that rests parallel to the undisturbed bed (10a) and an oscillatory component (11)

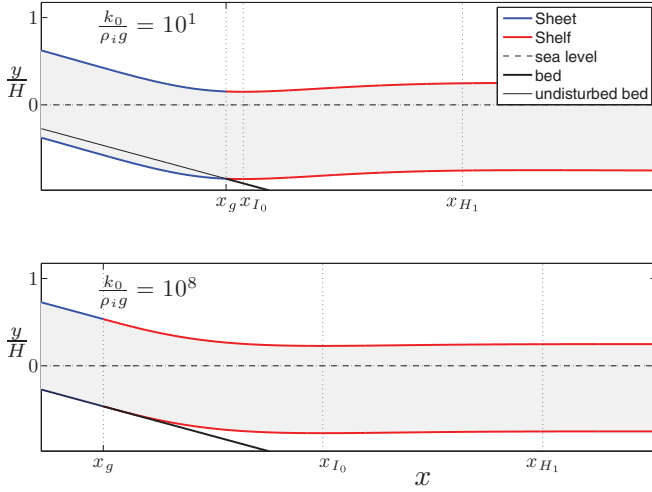


FIG. 3. (Color online) Deflection profile near the grounding line ($l/H \simeq 3.9$) with 3° bed slope, over a soft bed ($k_0/\rho_i g = 10$, top) and over a stiff bed ($k_0/\rho_i g = 10^8$, bottom), showing a grounding line below the ocean free surface. The sheet-shelf profile (blue and red, respectively) is marked by two curves that correspond to its surface and its bottom. The undisturbed bed profile is shown by a thick black line, and the sea surface is the dashed line, $y = 0$. The positions x_{I_0} and x_{H_1} are marked on each profile. Note that the soft bed below the sheet is depressed (top).

that decays exponentially as $x \rightarrow -\infty$ over a relaxation length $1/\gamma_0$ (8a). The solution for the floating shelf is

$$y_1 = \frac{1}{2} - \rho_{iw} + e^{-\gamma_1(x-x_g)} \left\{ \cos[\gamma_1(x-x_g)] \left(\rho_{iw} - \frac{Sx_g}{H} \right) - \frac{\sin[\gamma_1(x-x_g)]}{1 + \frac{\gamma_1}{\gamma_0}} \left[\frac{\gamma_0^2 \rho_i g}{\gamma_1^2 k_0} + \frac{\gamma_1}{\gamma_0} \left(\rho_{iw} - \frac{Sx_g}{H} \right) \right] \right\}, \quad (18)$$

which is a superposition of a free iceberg component (10b) and an oscillatory component (11) that decays exponentially as $x \rightarrow \infty$ over a relaxation length $1/\gamma_1$ (8b). These solutions (Fig. 3) and the deflection profiles for the case $x_g < 0$ (Fig. 4) indicate that the variation of the grounding-line position between a soft bed ($k_0/\rho_i g = 10$) and a stiffer bed ($k_0/\rho_i g = 10^8$) is comparable to the undulation length scale.

The grounding-line position corresponding to solutions (17) and (18) is determined by

$$x_g = \frac{H\rho_{iw}}{S} \left[1 + \left(\frac{\rho_w g}{k_0} \right)^{1/2} \right] - \frac{l\sqrt{2}}{1 + \left(\frac{\rho_w g}{k_0} \right)^{1/4}}, \quad (19)$$

which has two contributions: one proportional to $1/S$ due to the bed geometry and the other, proportional to l , due to the elastic deformations of the sheet and shelf. Both contributions also depend on the reaction modulus of the bed but in opposite ways. Specifically, on a softer bed the geometrical component is enhanced by the deforming elastic bed like $k_0^{-1/2}$, whereas the elastic component is weakened like $k_0^{-1/4}$, and vice versa on a stiffer bed. This behavior is emphasized when considering the grounding-line position in the limits of stiff and soft beds,

$$x_g = \begin{cases} \frac{H\rho_{iw}}{S} - l\sqrt{2}, & k_0 \rightarrow \infty \\ \frac{H\rho_{iw}}{S} \left(\frac{\rho_w g}{k_0} \right)^{1/2}, & k_0 \rightarrow 0 \end{cases}, \quad (20)$$

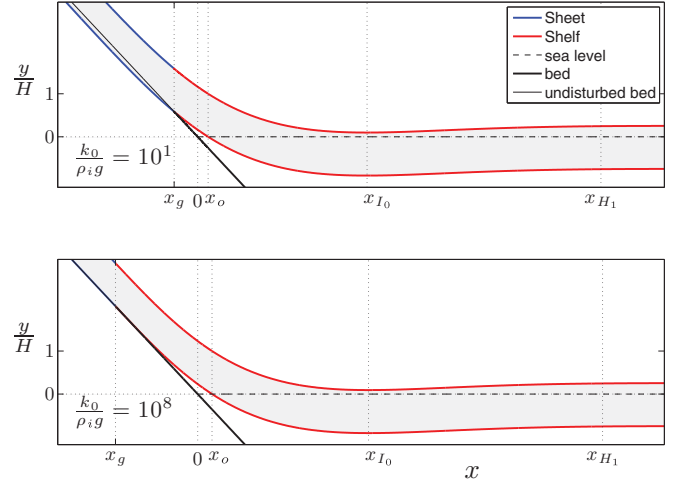


FIG. 4. (Color online) Deflection profile near the grounding line ($l/H \simeq 3.9$) with 24° bed slope, over a soft bed ($k_0/\rho_i g = 10$, top) and over a stiff bed ($k_0/\rho_i g = 10^8$, bottom), showing a grounding line above the ocean free surface. The interpretation of lines and symbols is similar to that in Fig. 3.

implying that the grounding-line position is much more sensitive to changes in the reaction modulus over soft beds than over stiff beds (Fig. 5).

It is also evident from (20) that in the stiff-bed limit the elastic contribution to the grounding-line position is maximal while it is negligible in the limit of soft beds. In particular, in the stiff bed limit of x_g the geometrical component balances the elastic one when $S = H\rho_{iw}/l\sqrt{2}$. Another situation where the elastic contribution can become insignificant is over shallow angles of the undisturbed bed.

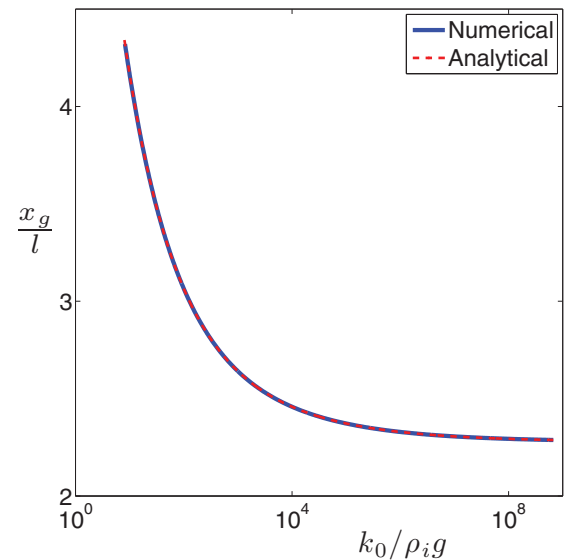


FIG. 5. (Color online) The grounding-line position x_g in units of the bending-buoyancy length scale l , as a function of the normalized reaction modulus of the bed for a bed slope 3° , obtained by numerical simulation (solid curve) and analytical solution (dashed curve).

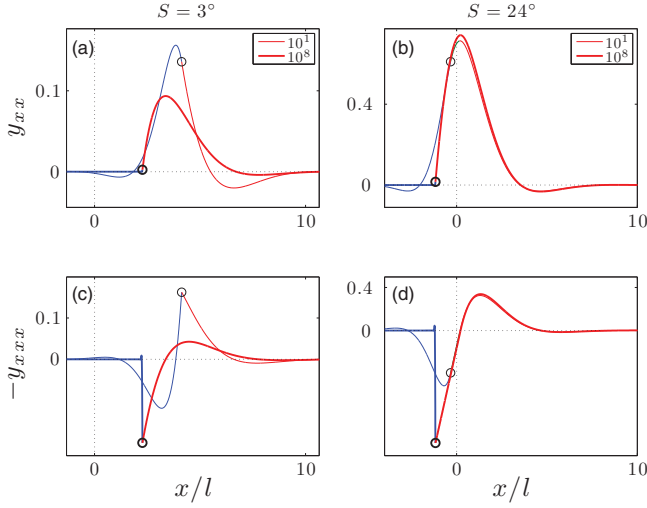


FIG. 6. (Color online) Dimensionless curvature y_{xx} , and the vertical shear force $-y_{xxx}$, of the solutions shown in Fig. 3 with bed slope 3° [(a) and (c)] and for the solutions shown in Fig. 4 with bed slope 24° [(b) and (d)]. Profile with thin line is over a soft bed ($k_0/\rho_i g = 10$), and thick line is over stiffer bed ($k_0/\rho_i g = 10^8$). The grounding-line positions are marked with \circ 's.

B. The curvature and shear force at the grounding line

The curvature and the shear force at the grounding line can vary substantially with the reaction modulus of the bed. In the long-shelf limit the curvature at the grounding line is

$$y_{xx}(x = x_g) = \frac{2\gamma_1^2}{1 + \frac{\gamma_1}{\gamma_0}} \left[\left(\frac{\gamma_0}{\gamma_1} \right)^2 \frac{\rho_i g}{k_0} + \frac{\gamma_1}{\gamma_0} \left(\rho_i w - \frac{Sx_g}{H} \right) \right], \quad (21)$$

which tends to zero in the limit of a stiff bed [Figs. 6(a) and 6(b)]. This behavior recovers the typical heavy elastica boundary condition, e.g. [19].

The shear force in the sheet is confined to a region near the grounding line of width that is proportional to $1/\gamma_0$ and narrows with the increase of the bed stiffness [Figs. 6(c) and 6(d)]. The confined shear force in the stiff bed limit reflects the sharp change in the reaction force on the sheet at the transition from a rigid bed support to an ocean support across the grounding line. However, in the asymptotic limit $k_0 \rightarrow \infty$ the model in Sec. II is no longer valid since $1/\gamma_0 \sim l/k_0^{1/4}$ becomes much smaller than the thickness H , implying that the region near the grounding line on the sheet side is no longer slender and therefore that the beam equations are no longer valid.

To study this asymptotic limit in a more complete model, we consider an elastic sheet having one region in contact with a horizontal and stiff surface and a blistered region that represents the shelf, with a grounding line in between at x_g . The full stress model for the grounded part of the sheet of length δ from the grounding line is,

$$\nabla \cdot \boldsymbol{\sigma} + \mathbf{F} = 0, \quad (22)$$

where $\boldsymbol{\sigma}$ is the stress tensor and \mathbf{F} is the net force due to gravity. We limit the analysis to the same spatial dimensions considered in Sec. II, so the force balance simplifies to

$$\sigma_{xx,x} + \sigma_{xy,y} = 0, \quad (23a)$$

$$\sigma_{yx,x} + \sigma_{yy,y} = \rho_i g, \quad (23b)$$

where x is the same as in Sec. II, y is the vertical coordinate, and the stress field is given by [20], equations [5.13],

$$\begin{aligned} \sigma_{xx} &= \frac{E}{(1+\nu)(1-2\nu)} [(1-\nu)\epsilon_{xx} + \nu\epsilon_{yy}], \\ \sigma_{yy} &= \frac{E}{(1+\nu)(1-2\nu)} [(1-\nu)\epsilon_{yy} + \nu\epsilon_{xx}], \\ \sigma_{yx} &= \frac{E}{1+\nu} \epsilon_{xy}, \end{aligned} \quad (24)$$

where $\epsilon_{xx} = u_{,x}$, $\epsilon_{yy} = w_{,y}$, and $\epsilon_{xy} = 1/2(u_{,y} + w_{,x})$ are the deformation tensor components. Equations (23) describe the stress balance in a boundary layer of width δ at the grounded side of the grounding line. Therefore, the boundary conditions at the grounding line (4c) should be satisfied when matching the solution to (23) with the outer solutions described in Sec. II. Our interest here is to use (23) to estimate δ . We define dimensionless variables,

$$\hat{y} = \frac{y}{H}, \quad \hat{x} = \frac{x_g - x}{\delta}, \quad \hat{u} = \frac{u}{U}, \quad \hat{w} = \frac{w}{W}, \quad (25)$$

where U and W are the scales for the horizontal and vertical deformations, respectively, and we get the dimensionless form of equations (23),

$$2(1-\nu) \frac{U}{\delta^2} u_{,xx} + (1-2\nu) \frac{U}{H^2} u_{,yy} - \frac{W}{H\delta} w_{,xy} = 0, \quad (26a)$$

$$2(1-\nu) \frac{W}{H^2} w_{,yy} + (1-2\nu) \frac{W}{\delta^2} w_{,xx} - \frac{U}{H\delta} u_{,xy} = -F_y, \quad (26b)$$

where all the hats were removed and $F_y = -2\rho_i g(1+\nu)(1-2\nu)/E$. We assume that the dominant balance in Eq. (26a) is determined by the first and last terms, namely that

$$\left[2(1-\nu) \frac{U}{\delta^2}, \frac{W}{H\delta} \right] \gg (1-2\nu) \frac{U}{H^2}, \quad (27)$$

which will prove to be consistent with the final result. Therefore, equating the dominant terms leads to

$$U \sim W \frac{\delta}{H} \frac{1}{2(1-\nu)}, \quad (28)$$

which simplifies Eq. (26b) to

$$2(1-\nu) \frac{W}{H^2} (w_{,yy} - u_{,xy}) + (1-2\nu) \frac{W}{\delta^2} w_{,xx} = -F_y. \quad (29)$$

In the absence of shear force at x_g , the second term on the left-hand side of (29) is negligible and the dominant balance is between the constant body force F_y and the first term. In the presence of a shear force, the second term becomes significant and therefore the only term that can vary and balance it is the first term. Therefore, the dominant balance is governed

by the left-hand side of (29), which leads to an explicit scale for the length scale δ ,

$$\delta = H \sqrt{\frac{1-2\nu}{2(1-\nu)}}, \quad (30)$$

which is consistent with the assumption at (27) for $\nu < 0.5$ (and in particular for $\nu \simeq 0.3$, the typical Poisson ratio for ice [21], p. 62). The limit (30) implies that the grounded sheet supports shear forces over a length scale that cannot be less than the order of the sheet's thickness. Hence, there is a critical reaction modulus k_c such that for all $k_0 \geq k_c$ that length scale does not change. We can evaluate k_c by balancing Eqs. (30) and (8a) to obtain

$$k_c = 16 \frac{D}{H^4} \left(\frac{1-\nu}{1-2\nu} \right)^2. \quad (31)$$

C. A shelf test for the bending-buoyancy length scale and bending stiffness

It is useful to find relations between the floating shelf deflection profile to the physical properties of the elastic sheet and the grounding-line position. Such relations could be applied to interpret geophysical data of ice sheets and ice shelves and to measure the bending-buoyancy length scale and the bending stiffness of an elastic sheet in a general context.

The length scale of the oscillatory pattern of the shelf is related to the bending-buoyancy length scale l [e.g., Eqs. (18) and (8b)]. In the limit of a long shelf, we can get an explicit relation for the positions of local minima or maxima in the shelf surface profile. Using (18), we find that the position of a local minimum or a local maximum in the shelf deflection is

$$x_I = x_g + l\sqrt{2} \tan^{-1} \left[\frac{\left(\frac{\gamma_0}{\gamma_1}\right)^2 \frac{\rho_i g}{k_0} + \left(\rho_{iw} - \frac{Sx_g}{H}\right) \left(1 + 2\frac{\gamma_1}{\gamma_0}\right)}{\left(\frac{\gamma_0}{\gamma_1}\right)^2 \frac{\rho_i g}{k_0} - \left(\rho_{iw} - \frac{Sx_g}{H}\right)} \right]. \quad (32)$$

In the limits of stiff and soft beds this simplifies to

$$x_{I_n} = \begin{cases} x_g + l\sqrt{2} \left(\frac{3\pi}{4} + n\pi\right), & k_0 \rightarrow \infty \\ x_g + l\sqrt{2} \left(\frac{5\pi}{4} + n\pi\right), & k_0 \rightarrow 0 \end{cases}, \quad (33)$$

where n is an integer index. Therefore, the interval between a local minimum and a consecutive local maximum is

$$d_{II} \equiv x_{I_{n+1}} - x_{I_n} = l\sqrt{2}\pi \quad (34)$$

in both limits, which is independent of both k_0 and the bed slope S . The bending stiffness of the sheet in terms of d_{II} is, therefore,

$$D = \rho_w g \left(\frac{\sqrt{2}}{2\pi} d_{II} \right)^4. \quad (35)$$

For the geophysical application a common observable is the position x_H , where the shelf surface elevation has the

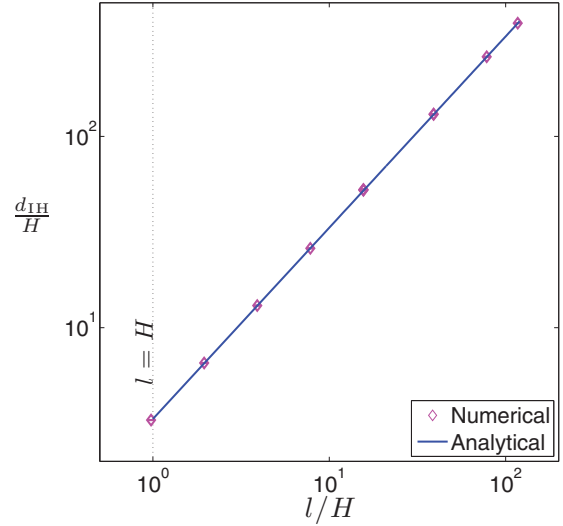


FIG. 7. (Color online) The dimensionless interval, d_{IH}/H as a function of l/H (log-log). Numerical values (\diamond) were computed for several bed slopes and over a range of bed stiffnesses $10 \leq k_0/\rho_i g \leq 10^8$, resulting in a variance smaller than 10^{-4} . Linear regression reveals a proportionality constant of 3.34, which differs by 0.3% from the theoretical value $l \frac{3\pi}{2\sqrt{2}}$ (line) in Eq. (38).

Archimedean value, satisfying $y(x_H) = 1/2 - \rho_{iw}$. Using the long-shelf limit (18),

$$x_H = x_g + l\sqrt{2} \tan^{-1} \left[\frac{\left(\rho_{iw} - \frac{Sx_g}{H}\right) \left(1 + \frac{\gamma_1}{\gamma_0}\right)}{\left(\frac{\gamma_0}{\gamma_1}\right)^2 \frac{\rho_i g}{k_0} + \frac{\gamma_1}{\gamma_0} \left(\rho_{iw} - \frac{Sx_g}{H}\right)} \right], \quad (36)$$

which in the limits of stiff and soft beds becomes

$$x_{H_n} = \begin{cases} x_g + l\sqrt{2} \left(\frac{\pi}{2} + n\pi\right), & k_0 \rightarrow \infty \\ x_g + l\sqrt{2} \left(\frac{5\pi}{4} + n\pi\right), & k_0 \rightarrow 0 \end{cases}, \quad (37)$$

implying that the surface elevation at the grounding line is not Archimedean in those limits. We can now calculate the interval d_{IH} between a local minimum and the nearest Archimedean position, which results in identical values at both stiff and soft bed limits and is given by

$$d_{IH} \equiv x_{H_1} - x_{I_0} = l \frac{3\pi}{2\sqrt{2}}, \quad (38)$$

implying that d_{IH} is independent of both k_0 and the bed slope S . The bending stiffness in terms of d_{IH} is

$$D = \rho_w g \left(\frac{2\sqrt{2}}{3\pi} d_{IH} \right)^4. \quad (39)$$

A numerical computation of d_{IH} is consistent with (38) in the range $10 \leq k_0/\rho_i g \leq 10^8$ and under variations of l and S (Fig. 7).

D. Finite shelf length

So far we have considered solutions in the asymptotic limit of a long shelf. The length of the shelf may become important when it is of the order of the bending-buoyancy length scale l . A finite shelf system includes the edge of the shelf x_s as an additional free boundary and hence the length constraint (5)

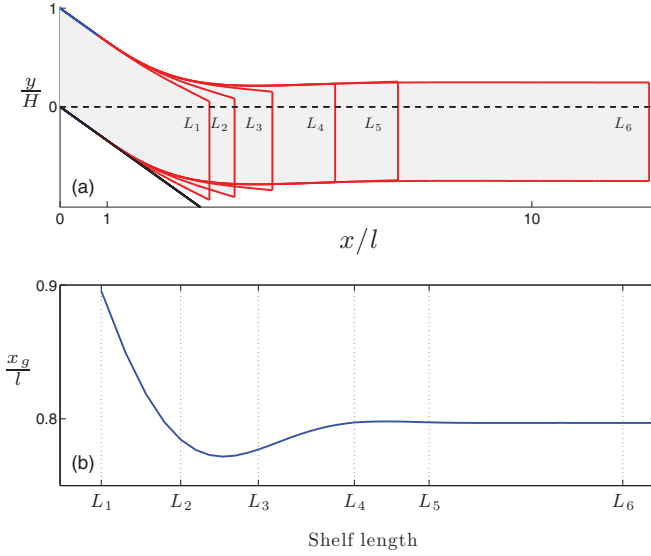


FIG. 8. (Color online) (a) Shelf profiles at the limit of stiff bed and with bed inclination of 3° , of the set lengths, $\{L_1, L_2, \dots, L_6\} \simeq \{2.3, 3.3, 3.7, 5, 6.4, 11.7\}l$. (b) The grounding-line position as a function of the shelf length (log scale) $L = \int_{x_g}^{x_s} \sqrt{1 + y'^2} dx$. The ticks $L_1 \dots L_6$ refer to the shelf profiles in (a).

as an additional boundary condition, which is nonlinear in y' . We therefore solve the finite shelf model numerically.

The models in Secs. II A and II B can be rescaled into the fixed domain $[0,1]$ by the mapping $\xi_i = \frac{x-x_i}{\Omega_i}$, where $i = 0,1$ for the model in Sec. II A with x_i representing x_f, x_g , respectively, and Ω_i are the intervals $x_g - x_f$ and $x_s - x_g$, respectively, and with a similar mapping for the model in Sec. II B but with an additional region due to extra free boundary at x_o . The rescaled model can then be rearranged to a set of algebraic equations for the coefficients a_{ij} and the free boundaries x_g, x_o, x_s , which are solved using the MATLAB optimization toolbox. To test the numerical simulation we compare its results with the analytical solution for the grounding-line position (19) under variation of the bed reaction modulus (Fig. 5) and variation of the bed slope and find good agreement between the two. Moreover, we find that (19), which was developed for the case $x_g > 0$ accounts also for the case where $x_g < 0$ over stiff beds with angles less than $\sim 15^\circ$ and over soft beds.

The numerical results for the deflection profile [Fig. 8(a)] and for the grounding-line position [Fig. 8(b)] suggest that the length of the shelf becomes relevant to the solution when it is of the order of the bending-buoyancy length scale l . For example, the response of the grounding line is negligible as long as $L > L_4 = 5l$, while it is about 10% of l when the shelf length drops by 50% between L_4 to L_1 [Fig. 8(b)].

IV. EXPERIMENTS

To validate some of the theoretical results, we set up an experiment to measure the grounding-line position x_g and the position of the first local minimum in the shelf profile x_{l_0} as functions of bed slope.

To represent an elastic sheet-shelf we used two different bands of silicone rubber having dimensions of $120 \times 4 \times$

TABLE I. Parameters of the elastic sheets used in the experiments.

Physical quantity	Symbol	Values	Units
Sheet density	ρ_i	1.14	g/cm^3
Sheet thickness	H	0.93 1.92	cm
Loop height	y_M	7.4 11.8	cm
Bending stiffness	D	0.566 4.744	10^6 gm(cm/s)^2

1 cm and $120 \times 8 \times 2$ cm and density $\rho_i \simeq 1.14 \text{ gm/cm}^3$. The bands were prepared by mixing two fluid components ('Zhermack and Elite Double 22) and leaving the mixture to polymerize inside a mold of high precision so the thicknesses of the sheets were uniform to within ± 0.1 mm. To measure the bending stiffness D , defined in (2), the rubber sheets were placed on a flat, rigid surface where one end was coiled to form a loop so its edge was placed back parallel to the flat surface. The maximum height of the loop y_M is related to the stiffness of the sheet by [22]

$$l_i = 1.103 y_M, \quad (40)$$

where $l_i = (D/\rho_i g H)^{1/3}$, which implies (Table I) that $E^* \simeq 0.845 \text{ MPa}$ for the thin sheet and $E^* \simeq 0.804 \text{ MPa}$ for the thicker one, where $E^* \equiv E/(1 - \nu^2)$. This $\sim 5\%$ difference possibly resulted from nonuniformities in volume ratio and quality of mixing of the two components in the molding procedure. To represent the ocean, we used a potassium-carbonate salt solution of two different concentrations (Table II).

The elastic sheets and the salt solution were contained inside an acrylic rectangular tank of dimensions $200 \times 20 \times 25$ cm, with an opaque base. The tank was mounted on a rigid, flat surface that had adjustable inclination (Figs. 9 and 1). We used a laser sheet mounted to a traversing platform to measure the deflection profile of the elastic sheet, the bed slope, and the position of the ‘‘coast’’ (intersection of the ocean, the tank base, and air). The laser sheet was aligned perpendicularly to the long axis of the tank and had a sampling rate of 25 s^{-1} and accuracy of 0.1 mm. The traversing platform traveled parallel to the long axis of the tank at 25 mm s^{-1} . This resulted in a total spatial resolution of 1 mm along the long axis of the elastic sheet. The length of the projected laser sheet on the tank surface was about 12 cm so the range it captured included the entire width of the elastic sheet and either the bottom surface of the tank or the ocean surface.

We performed four sets of experiments using elastic sheets of two different thicknesses and ocean solutions of two different densities (Table II). In each experiment we measured the deflection profile of the sheet surface for a set of inclinations ranging from $\sim 2^\circ$ to about 15° in intervals

TABLE II. Experiment parameters and regression results.

Expt.	H (cm)	ρ_w (g/cm^3)	$H\rho_{iw}$ (cm)	C_1 (cm)	$l\sqrt{2}$ (cm)	C_2 (cm)
1a	0.93	1.534	0.693	0.711	6.23	6.80
1b	0.93	1.202	0.884	1.021	6.62	7.69
2a	1.92	1.532	1.432	1.477	10.6	11.04
2b	1.92	1.202	1.825	1.711	11.26	10.8

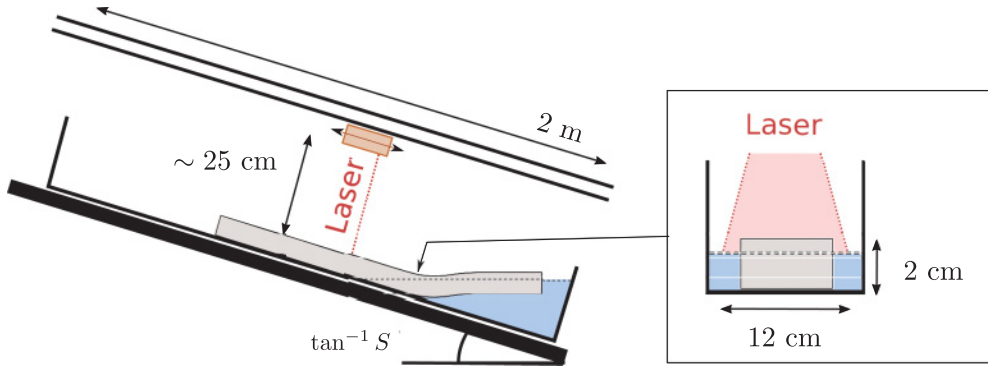


FIG. 9. (Color online) Experimental apparatus to measure $x_g(S)$ and x_{I_0} . A rigid tank, 2 m long, was mounted to a flat surface with adjustable inclination. An elastic sheet made of silicone rubber was placed inside the tank, and a potassium-carbonate solution denser than the sheet partially filled the tank. A laser sheet was mounted to a platform that can move parallel to the tank and measure the deflection of the elastic sheet. The inset diagram is a vertical cross section, transverse to the sheet long axis at the position marked by the arrow, showing a grounded part of the elastic sheet, the surrounding ocean, and the laser sheet.

of 0.2 to 0.5°. Each experiment started by setting the tank at the largest inclination and adding the potassium-carbonate solution. An elastic sheet was then placed on the tank surface so a little more than $4l$ of the sheet’s length was supported by the liquid and the rest by the solid surface of the tank. This was to diminish the effect of the shelf length on the grounding-line position. The inside of the tank was then scanned by the laser sheet and the two-dimensional laser reading was stored in a data file. Then the procedure of reducing the tank inclination and scanning was repeated.

The data was later processed to produce two curves; the elevation of the elastic sheet surface $h'(x')$, and the elevation of the surface surrounding the sheet $b'(x')$, which included the tank surface and the ocean surface (primes mark quantities in the reference frame of the tank). Those curves were generated by splitting the data at each position x' along the sheet into two

segments and then averaging each segment. The curve $b'(x')$ was used to extract the bed slope $\tan^{-1} S$ and the position of the coast, which defines the origin $x' = x = 0$. We used those values to compute the deflection profile $y(x)$ in the reference frame of the laboratory.

The technique to resolve the grounding-line position given $y(x)$ was based on the theoretical result that the curvature of the sheet at the grounding line is negligible (Sec. III B) compared to that of the shelf near the grounding line in the limit of stiff bed. We first obtained the curvature y_{xx} and then computed a piecewise regression to the theoretical curvature function. More specifically, the curvature was obtained by differencing $y(x)$ twice; however, this operation significantly reduced the signal-to-noise ratio, so we overcame that by dividing the deflection data into a set of consecutive intervals, 2 cm long, and fitted to each interval n a parabolic profile, $y_n = A_n x^2 + B_n x + C_n$, where the capitals represent the fitted parameters. The curvature at that interval was then defined as $\kappa_n = 2A_n$, so the set $\kappa(x) \equiv \{\kappa_n\}$ represented the measured curvature of the elastic sheet. Next, we used the theoretical curvature derived from the solutions to Eqs. (31) and (12) as a regression function, where the coefficients a_{ij} were determined by the boundary conditions as in Sec. II, and the positions x_g, x_o, x_s and the coefficients $\gamma_{0,1,2}$ and $\bar{\gamma}_1$ were the free parameters of the regression [e.g., Fig. 10(a)]. We verified that the free parameters converged to reasonable values by comparing the theoretical deflection profile to the one resulting from the regression [e.g., Fig. 10(b)].

We note that the deflection profile we measured was of the elastic sheet surface. Consistency with slender beam theory required to extrapolate the measured deflection profile to the midsurface of the sheet. This correction had two contributions. First, the position of edge of the sheet surface (x_f, y_f) was translated to the midsurface $(x_f - \frac{1}{2}HS/\sqrt{1+S^2}, y_f - \frac{1}{2}H\sqrt{1+S^2})$. Then an arclength element at the sheet surface ds was adjusted to the corresponding arc-length element at the midsurface $\bar{d}s$ according to $\bar{d}s_n = ds_n(1 + \frac{1}{2}H\kappa_n)$.

The results of the data analysis is a graph, $x_g(S)$, for each of the four experiments in Table II. We then used the theoretical prediction, Eq. (20) as a regression function, $x_g(S) = C_1/S - C_2$, where $C_{1,2}$ are free parameters. The

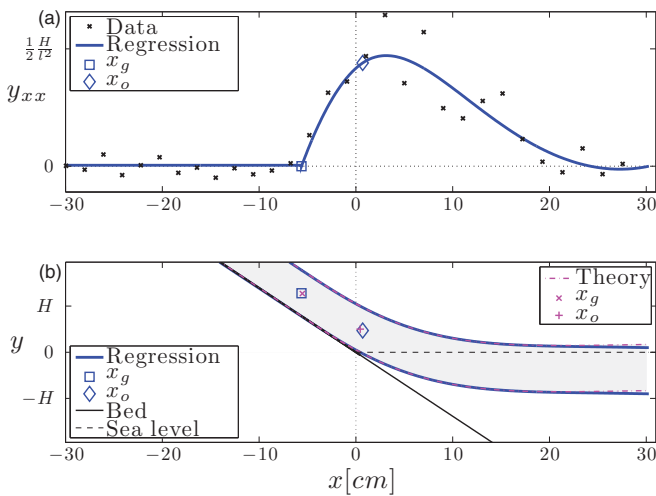


FIG. 10. (Color online) (a) The regression result of the theoretical curvature (line) to the curvature derived from the measured deflection profile (\times). (b) The corresponding deflection profile based on the fitted parameters (line) compared with the theoretical prediction (dash-dot), validating that the other regression fitting parameters converged properly. Bed inclination is 14.9° and the experiment parameters are of line 2a in Table II.

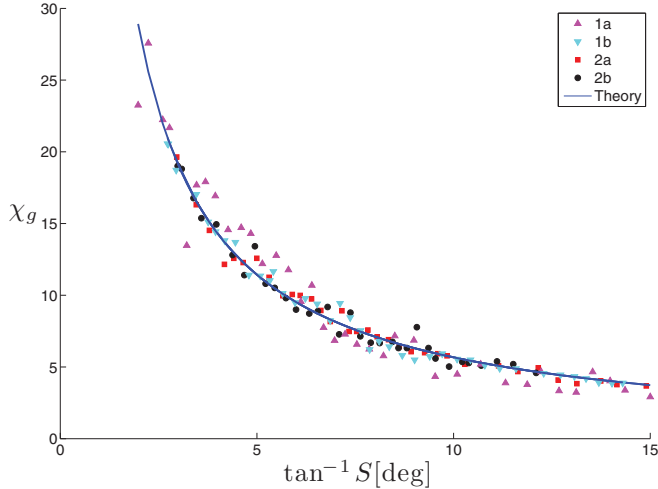


FIG. 11. (Color online) Experimental data and theoretical prediction of the dimensionless grounding line χ_g as a function of the bed inclination [Eq. (41)]. The data were produced from four experiments where the elastic sheet thickness and the ocean density were varied (Table II).

grounding-line position was then nondimensionalized by writing

$$\chi_g = (x_g + C_2)/C_1, \quad (41)$$

such that all the data collapsed into a single curve shown in Fig. 11. Comparing the regression results to the theoretical values of $C_{1,2}$ (Table II) indicated errors of less than 7% for the thicker elastic sheet, whereas the thinner sheet experiments had errors of less than 14%.

To demonstrate that our experimental apparatus is sensitive to the elastic contribution to the grounding-line position $l\sqrt{2}$, we eliminate the geometrical contribution to the grounding-line position, denoted as x'_g , from the experimental data (Fig. 12, bottom). The result indicates that most of the experimental data embeds a clear signal of the elastic contribution to the grounding-line position to within 10% of the predicted value. A larger discrepancy is present in experiment 1a at the range of lower angles.

Another confirmation of the theory was obtained by measuring the position of the nearest local minimum to the grounding line, x_{I_0} . The calculation of this position was performed by computing the first derivative of the deflection data and then interpolating a curve using four data points nearest to where the slope first vanishes after the grounding-line position. Comparing the value of interval $x_{I_0} - x_g$ to the theoretical prediction of $l3\pi/2\sqrt{2}$ (33) demonstrates a good agreement (Fig. 12, top).

The agreement within acceptable uncertainty between the experiments and the theory in Figs. 11 and 12 was achieved without having to account for surface forces such as van der Waals adhesion of the sheet to the tank surface or surface tension. These surface effects are less important compared to the body forces for the materials we use owing to the large sheet thickness. Specifically, when the sheet is in full contact with a stiff and flat bed its total energy is a sum of gravitational energy \mathcal{U}_g and surface energy \mathcal{U}_s . Bending energy in that case

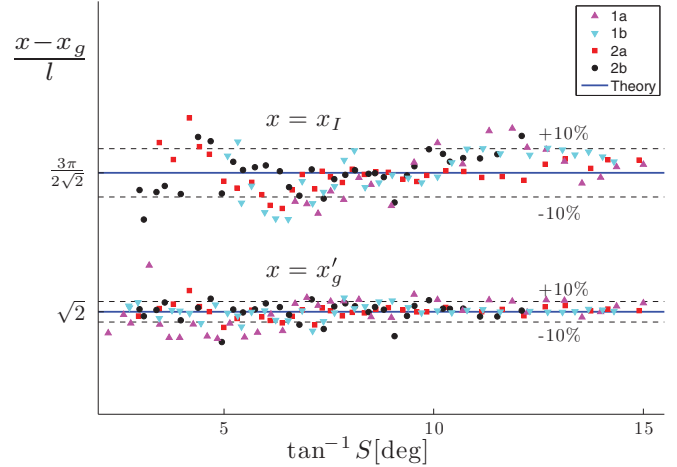


FIG. 12. (Color online) The difference between the geometrical component of the grounding-line position x'_g and the grounding line x_g , normalized by the bending-buoyancy length scale l , compared with the predicted value in Eq. (20), and the interval between the grounding line and the nearest local minimum normalized by l , compared with the predicted value in Eq. (33) (experimental data at Table II). Dash lines represent $\pm 10\%$ departures from the theoretical values.

is zero as there is no curvature. If the interface has surface area A then by order of magnitude $\mathcal{U}_g/A = \rho_i g h^2 \simeq 1 \text{ J m}^{-2}$ (Table I). The surface energy per unit area is $\mathcal{U}_s/A = \Delta\gamma$, where $\Delta\gamma$ is the interfacial toughness, which for the elastomer we use a typical value is 0.1 J m^{-2} [23]. Therefore $\mathcal{U}_g \gg \mathcal{U}_s$ and so to leading order the surface energy can be neglected.

V. SUMMARY AND CONCLUSIONS

We have presented a theoretical and experimental analysis of a grounded elastic sheet coupled to a floating elastic shelf, motivated by similar systems of ice sheets and ice shelves observed in polar regions. In particular, we modelled the grounding line as a free boundary and the bed beneath the grounded sheet with variable softness. Our analysis focused on the dynamics near and at the grounding line and on the relation between the structure of the shelf to the physical properties of the system and to the grounding-line position.

In the long-shelf limit we found analytical solutions for the deflection profile and the grounding-line position. Specifically, the grounding-line position has two contributions, due to the geometry of the bed and to the bending-buoyancy length scale, which encapsulates the bending stiffness of the elastic sheet and the reaction force due to the denser ocean. These two contributions depend on the bed reaction modulus in opposite ways so the geometrical component tends to diminish over a stiffer bed while the elastic component intensifies. We showed that the curvature at the grounding line tends to zero in the limit of a stiff bed and that the shear force within the grounded sheet is confined into an increasingly narrow layer near the grounding line as the bed stiffens. In particular, ice elevation at the grounding line does not necessarily satisfy the Archimedean balance due to the nonzero shear force there. We also showed that ice bending stiffness can be computed

directly from measurable intervals on the surface of the shelf, such as the interval between a local minimum in the deflection and the nearest Archimedean position, and that this quantity is independent of the bed structure or stiffness. We also presented explicit relations between the grounding-line position and measurable positions on the undulated shelf. Numerical computations indicated that the length of the shelf has a small effect on the solution, and that it becomes important when it is of the same order of magnitude as the bending-buoyancy length scale. We then showed consistency of some theoretical results with laboratory scale experiments using silicone rubber sheets and dense salt solutions.

This study provides a practical method to measure the bending stiffness and bending-buoyancy length scale of elastic sheets directly from the geometrical characteristics of the

floating shelf. In particular this method can be used to study the elastic properties of ice sheets using available satellite data and to put better constraints on the grounding-line position and on the properties of the bed beneath the grounded sheet.

ACKNOWLEDGMENTS

We thank Herbert Huppert and Dominic Vella for their comments on an early version of this manuscript. We thank John Lister, Jerome Neufeld, and Dominic Vella for useful discussions. We thank Jim McElwaine for the use of his inclined surface and laser sheet, Mark Hallworth for his assistance in producing the images in Fig. 1, and the technicians of the Batchelor fluid laboratory. R.S. acknowledges the support of NERC.

-
- [1] T. Hughes, *J. Geophys. Res.* **78**, 7884 (1973).
 - [2] N. Iverson, R. Baker, R. Hooke, B. Hanson, and P. Jansson, *J. Glaciol.* **45**, 31 (1999).
 - [3] H. A. Fricker and L. Padman, *Geophys. Res. Lett.* **33**, L15502 (2006).
 - [4] A. Wilchinsky and V. Chugunov, *J. Appl. Maths Mechs* **65**, 479 (2001).
 - [5] S. Nowicki and D. Wingham, *Earth Planet. Sci. Lett.* **265**, 246 (2008).
 - [6] G. Durand, O. Gagliardini, B. de Fleurian, T. Zwinger, and E. Le Meur, *J. Geophys. Res.-Earth* **114**, F03009 (2009).
 - [7] C. Schoof, *J. Fluid Mech.* **679**, 122 (2011).
 - [8] G. Holdsworth, *J. Glaciol.* **8**, 385 (1969).
 - [9] G. Holdsworth, *Ann. Geophys.* **33**, 133 (1977).
 - [10] T. Hughes, *Rev. Geophys.* **15**, 1 (1977).
 - [11] D. G. Vaughan, *J. Geophys. Res.-Sol. Ea.* **100**, 6213 (1995).
 - [12] N. Reeh, E. Christensen, C. Mayer, and O. Olesen, *Ann. Glaciol.* **37**, 83 (2003).
 - [13] R. Sayag and M. G. Worster (in preparation, 2011).
 - [14] M. G. Worster, in *Perspectives in Fluid Dynamics*, edited by G. K. Batchelor, H. K. Moffatt, and M. G. Worster (Cambridge University Press, New York, 2000), Chap. 8.
 - [15] J. Weertman, *J. Glaciol.* **13**, 3 (1974).
 - [16] C. Schoof, *J. Fluid Mech.* **573**, 27 (2007).
 - [17] R. A. V. Robison, H. E. Huppert, and M. G. Worster, *J. Fluid Mech.* **648**, 363 (2010).
 - [18] A. Boresi and R. Schmidt, *Advanced Mechanics of Materials*, 6th ed. (Wiley, New York, 2003).
 - [19] C. Wang, *Int. J. Mech. Sci.* **28**, 549 (1986).
 - [20] L. Landau and E. Lifshitz, *Theory of Elasticity*, 2nd ed. (Pergamon Press, 1970), Vol. 7.
 - [21] K. Hutter, *Theoretical Glaciology* (D. Reidel, Dordrecht, 1983).
 - [22] Stuart, *Br. J. Appl. Phys.* **17**, 1215 (1966).
 - [23] D. Vella, J. Bico, A. Boudaoud, B. Roman, and P. M. Reis, *Proc. Natl. Acad. Sci. USA* **106**, 10901 (2009).